Journal of
Marine Science and Engineering

Review

Development History of the Numerical Simulation of Tides in the East Asian Marginal Seas: An Overview

Zexun Wei [1,2,3,*], Haidong Pan [1,2,3], Tengfei Xu [1,2,3], Yonggang Wang [1,2,3] and Jian Wang [1,2,3]

1 First Institute of Oceanography, and Key Laboratory of Marine Science and Numerical Modeling, Ministry of Natural Resources, Qingdao 266061, China; panhaidong@fio.org.cn (H.P.); xutengfei@fio.org.cn (T.X.); ygwang@fio.org.cn (Y.W.); wangjian_upc@163.com (J.W.)
2 Laboratory for Regional Oceanography and Numerical Modeling, Pilot National Laboratory for Marine Science and Technology, Qingdao 266237, China
3 Shandong Key Laboratory of Marine Science and Numerical Modeling, Qingdao 266061, China
* Correspondence: weizx@fio.org.cn

Abstract: As a ubiquitous movement in the ocean, tides are vital for marine life and numerous marine activities such as fishing and ocean engineering. Tidal dynamics are complicated in the East Asian marginal seas (EAMS) due to changing complex topography and coastlines related to human activities (e.g., land reclamation and channel deepening) and natural variability (e.g., seasonal variations of ocean stratification and river flow). As an important tool, numerical models are widely used because they can provide basin-scale patterns of tidal dynamics compared to point-based tide gauges. This paper aims to overview the development history of the numerical simulation of tides in the EAMS, including the Bohai Sea, the Yellow Sea, the East China Sea, the East/Japan Sea, and the South China Sea, provide comprehensive understanding of tidal dynamics, and address contemporary research challenges. The basic features of major tidal constituents obtained by tidal models are reviewed, and the progress in the inversion of spatially and temporally changing model parameters via the adjoint method are presented. We review numerical research on how a changing ocean environment induces tidal evolution and how tides and tidal mixing influence ocean environment in turn. The generation, propagation, and dissipation of internal tides in the EAMS are also reviewed. Although remarkable progresses in tidal dynamics have been made, nonstationary tidal variations are not fully explained yet, and further efforts are needed. In addition, tidal influences on ocean environment still receive limited attention, which deserves special attention.

Keywords: tides; ocean model; South China Sea; East China Sea; adjoint assimilation method; internal tides; tidal mixing

check for updates

Citation: Wei, Z.; Pan, H.; Xu, T.; Wang, Y.; Wang, J. Development History of the Numerical Simulation of Tides in the East Asian Marginal Seas: An Overview. *J. Mar. Sci. Eng.* **2022**, *10*, 984. https://doi.org/10.3390/jmse10070984

Academic Editors: Marco Petti, Han Soo Lee, Kyeong Ok Kim, Seung-Buhm Woo, Jin-Hee Yuk and Youngjin Choi

Received: 30 June 2022
Accepted: 13 July 2022
Published: 19 July 2022

Publisher's Note: MDPI stays neutral with regard to jurisdictional claims in published maps and institutional affiliations.

Copyright: © 2022 by the authors. Licensee MDPI, Basel, Switzerland. This article is an open access article distributed under the terms and conditions of the Creative Commons Attribution (CC BY) license (https://creativecommons.org/licenses/by/4.0/).

1. Introduction

Tides are periodic sea level oscillations originated from the gravitation of the moon and the sun [1]. Tides are ubiquitous in the global ocean, and the accurate prediction of tides is essential and necessary for marine activities such as fishing, ocean transport, and ocean engineering [2]. East Asian marginal seas (EAMS), including the Bohai Sea, the Yellow Sea, the East China Sea, the East/Japan Sea, and the South China Sea, have complicated topography and coastlines that induce complex tidal dynamics [3,4]. In most locations in the EAMS, the strongest tidal constituent is M_2 with a period of 12.4206 h. Other significant semi-diurnal tides include S_2 (12 h), K_2 (11.9672 h), and N_2 (12.6583 h). In minor locations such as the Gulf of Tonkin, diurnal tides like K_1 (23.9345 h) and O_1 (25.8193 h) are stronger than M_2 tides. Because of relatively shallow water depth, tidal ranges in the EAMS are significantly larger than those in deep seas, for example, at Incheon in the Yellow Sea, the local tidal range can exceed 10 m [5,6]. Furthermore, due to the rapid development of economy and thus increasing human activities, such as harbor construction, land reclamation, and channel deepening, local coastlines and topography have been significantly changed, which contributes to local tidal evolution [7–9].

Based on tide gauges, satellite altimeter observations and numerical models, numerous studies have been conducted in the EAMS, revealing basic features of major tidal constituents and exploring multi-time scale tidal evolution [10–13]. The purpose of this paper is to overview the development history of the numerical simulation of tides in the EAMS, provide comprehensive understanding of tidal dynamics, and address contemporary research challenges. Compared to point-based tide gauge observations, numerical models can provide basin-scale patterns of tidal dynamics. Before the 1990s, due to the limitation of computer power, ocean tide models were mainly two-dimensional (2D), and their resolution was relatively low. High-resolution three-dimensional (3D) tidal models have gradually become common since the 1990s as the result of improved computer power. The rapid increase of satellite observations since the 1990s popularized the assimilated tidal models, which significantly improved the accuracy of tidal models in the sea area with rare tide gauges [14,15]. Alongside simulating accurate tidal constants, numerous studies also focus on exploring nonstationary tidal amplitudes/phases' changes caused by human activities and natural variability (e.g., seasonal variations of ocean stratification and river flow). As a typical nonstationary tide, internal tides receive lots of attention, especially in the South China Sea [16–18]. In addition, recent studies indicate the importance of tides and tidal mixing on influencing the ocean environment and global climate [19–21].

The structure of this paper is as follows. In Section 2, we review numerical research on stationary tides in the EAMS via 2D and 3D models without data assimilation. In Section 3, we review numerical studies using an assimilated tidal model and the progress in the inversion of spatially and temporally changing model parameters. The interactions between the ocean environment and tides is discussed in Sections 4 and 5. Numerical studies on internal tides are described in Section 6. Summary and conclusions are given in Section 7.

2. Tidal Modeling without Data Assimilation

In early numerical studies, due to lack of computer resources, most research simulated tides using 2D tidal models. Numerically simulated M_2 tides in the Bohai and Yellow Seas (BYS) indicated that bottom friction is vital in shallow water, and semi-diurnal tides in the coast of the Korean Peninsula are noticeably larger than those in the coast of China [10] (Figure 1). Via numerical modeling, Shen [5] obtained the co-tidal charts of M_2, S_2, K_1, and O_1 tides in the East China Sea which are consistent with observations. As shown in Figure 1, for the M_2 tide, there exist four amphidromic points in the BYS: two amphidromic points located in the Bohai Sea, one near Qinhuangdao (labeled as Q in Figure 1), and another located in the Yellow River delta (labeled as Y); two amphidromic points located in the Yellow Sea, one located in the north of Chengshantou (labeled as C), and another located in the east of Jiangsu coast (labeled as J). For the K_1 tide, there are only two amphidromic points in the BYS, one is located in the Bohai Strait (labeled as B in Figure 2), and the other lies in the middle of the South Yellow Sea (labeled as S).

Fang [22] modeled the tides and tidal currents in the Taiwan Strait using 2D nonlinear hydrodynamic equations and concluded that most of the energy flux of semi-diurnal tides in the Taiwan Strait is from the East China Sea. Fang and Yang [23] simultaneously simulated semi-diurnal, diurnal, and shallow-water tidal constituents as well as tidal currents in the Bohai Sea based on 2D tidal wave equations. Fang [24] proposed a finite difference–least square technique to solve tidal wave equations and applied this technique to model the M_2 tide in the Yellow Sea. Via numerical modeling, Fang [25] gave the charts for tides and tidal currents in the marginal seas adjacent to China. In fact, these experiments were performed in 1970s, but the results remained unpublished for many years because of the fact that the publication of Chinese scientific journals had been halted during that time. Fang and Yang [26] computed semi-diurnal and diurnal tides and tidal currents in the Korea Strait and proposed a method for large-area tides and tidal currents' prediction.

Odamaki [27] explored the generation mechanism of tides in the East/Japan Sea by means of a one-dimensional tidal model. He found that semi-diurnal and diurnal tides in the East/Japan Sea are generally weak, and most tidal energy was from the Korea Strait (Figure 3). Cao and Fang [28] simulated diurnal and semi-diurnal tides and tidal currents in the Gulf of Tonkin and gave the distribution of the tidal energy flux, the residual tidal current, and the residual tidal elevation. As displayed in Figure 4, K_1 amplitudes in the Gulf of Tonkin can reach 80 cm, while the maximum of M_2 amplitudes is only about 30 cm. Choi and Fang [29] reviewed earlier numerical studies of the Bohai, Yellow, and East China Seas (BYECS) and discussed the utilization of numerical models to study tidal mixing, tidal circulation, and tidal sedimentation. Zhao et al. [30] discussed the characteristics of tidal residual currents in the BYECS and found that the directions of tidal residual currents are consistent with the coastal current system in most areas. Fang et al. [31] simulated principal tidal constituents in the South China Sea and confirmed that a clockwise rotating M_2 amphidromic point located in the southeast of the Gulf of Thailand (labeled as M in Figure 5) and a counterclockwise rotating K_1 amphidromic point lied in the south of the Gulf of Thailand (labeled as K in Figure 4).

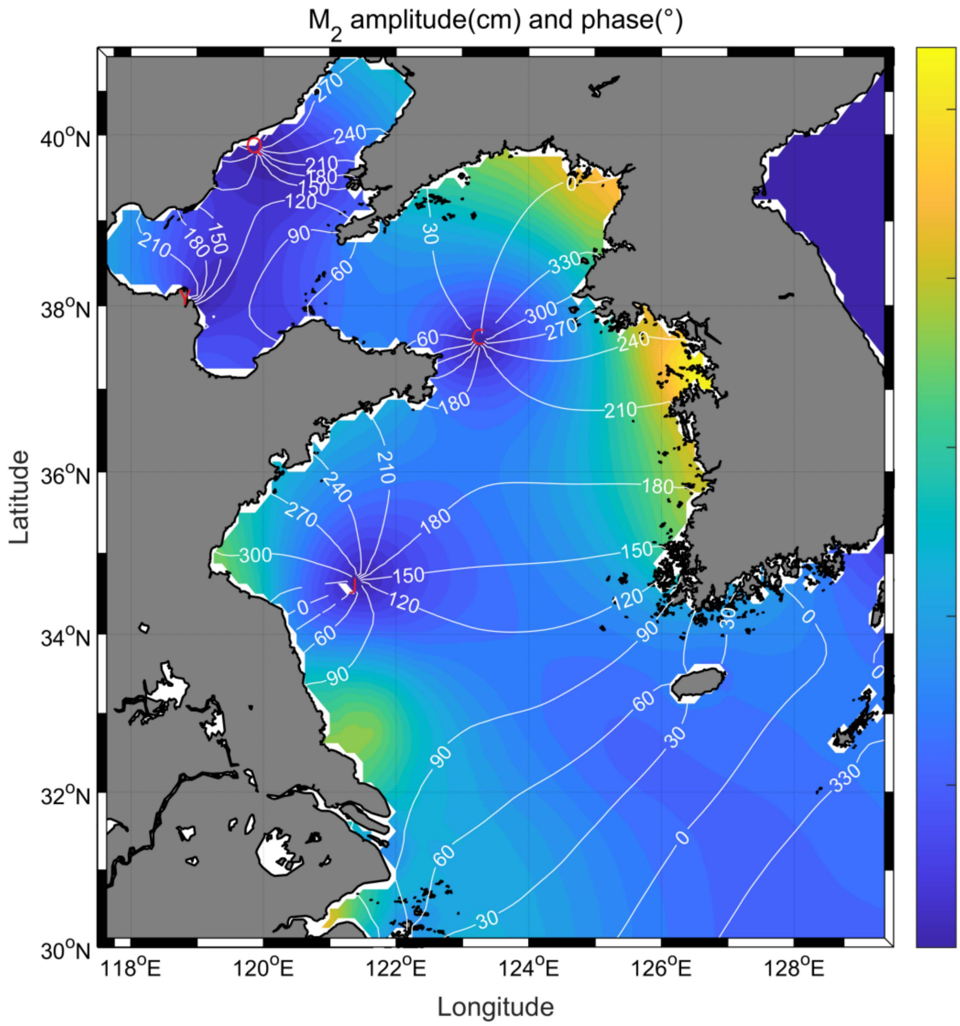

Figure 1. Cotidal chart for M_2 in the BYS based on the EOT20 model [32], in which the color and white lines represent the amplitude and phase lag, respectively.

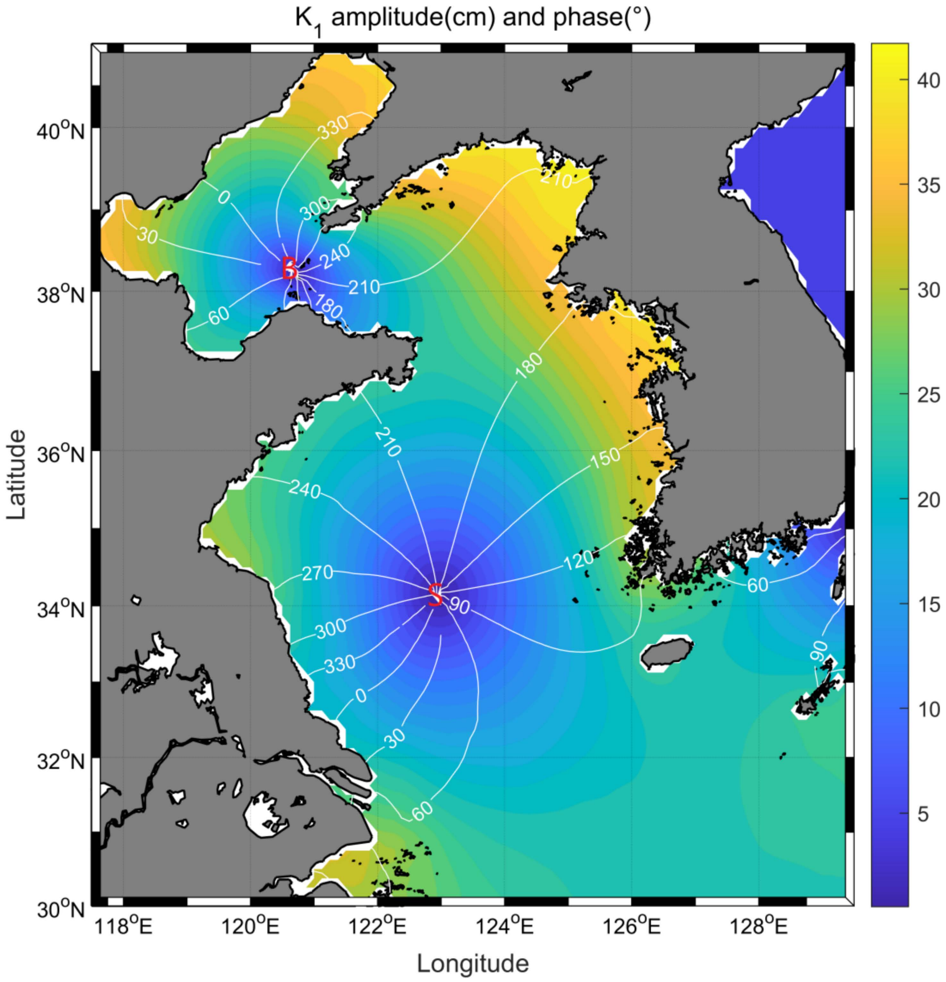

Figure 2. Same as Figure 1, but for the K_1 tide.

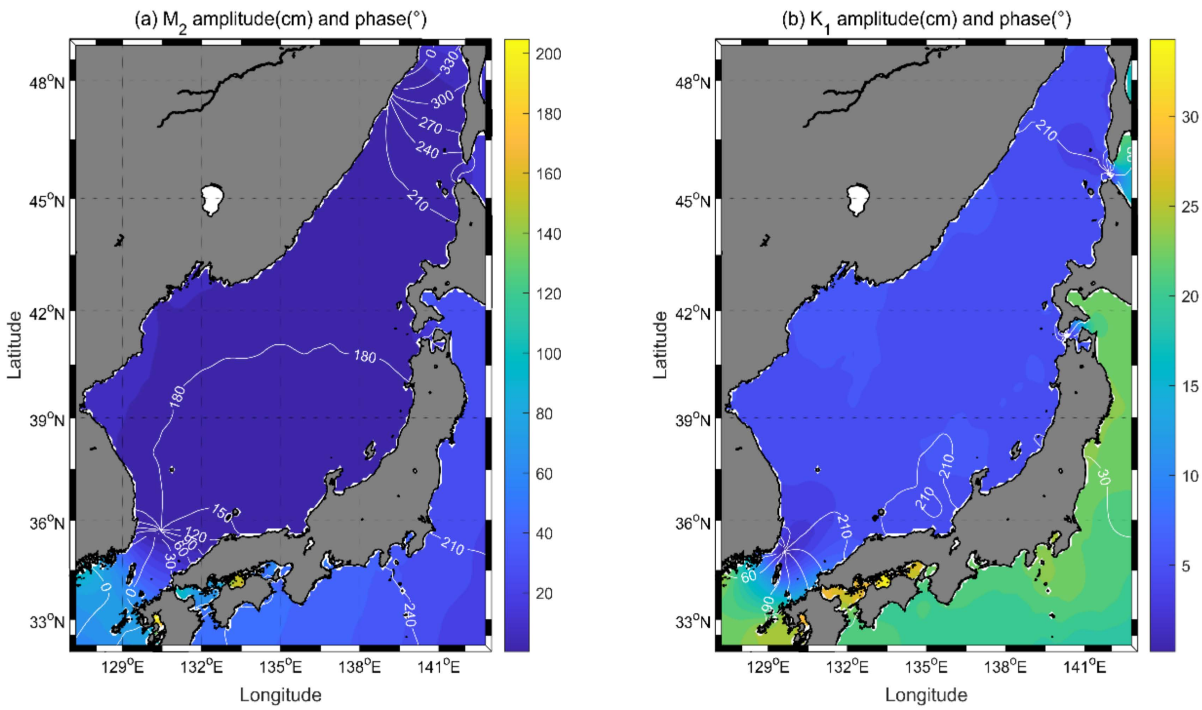

Figure 3. Cotidal charts for M_2 (**a**) and K_1 (**b**) tides in the East/Japan Sea.

Using a 2D finite element model, Lin et al. [33] indicated that the anomalous amplifications of semi-diurnal tides along the western coast of Taiwan (Figure 6) are caused by resonance. Jan et al. [34] found the importance of the abrupt step in the topography to the amplification of semi-diurnal tides in the Taiwan Strait based on numerical experiments and theoretical analysis. Teng et al. [35] considered the effects of self-attraction loading and internal tide dissipation to M_2 and S_2 tides in the BYECS and found that 80% of tidal energy was dissipated via bottom friction and the remaining 20% was dissipated via internal tide dissipation. Zhang et al. [36] designed a schematized numerical tidal model to investigate the generation of tidal current system in the Yellow Sea and concluded that Poincare modes were necessary for the existence of the radial tidal current.

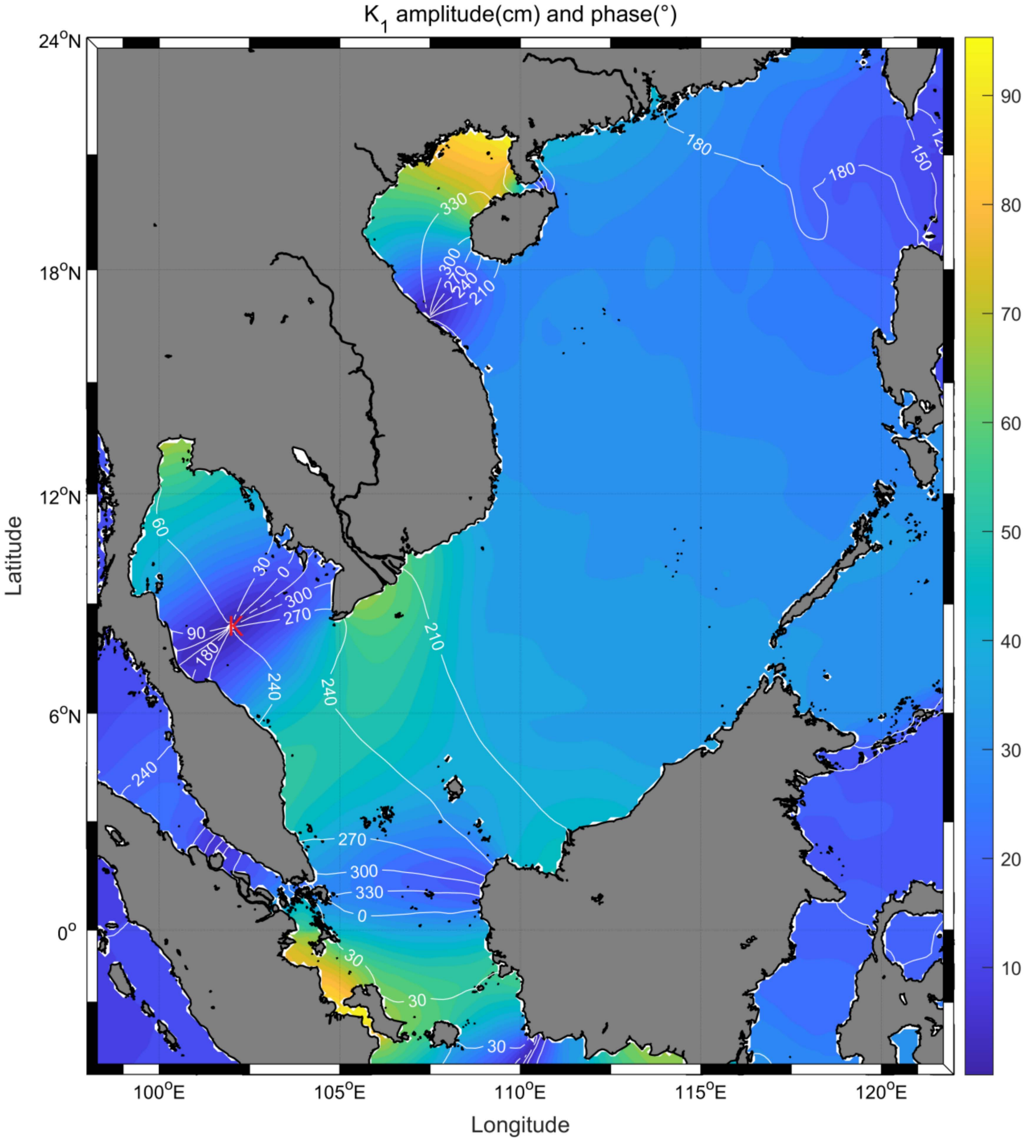

Figure 4. Same as Figure 2, but for the South China Sea.

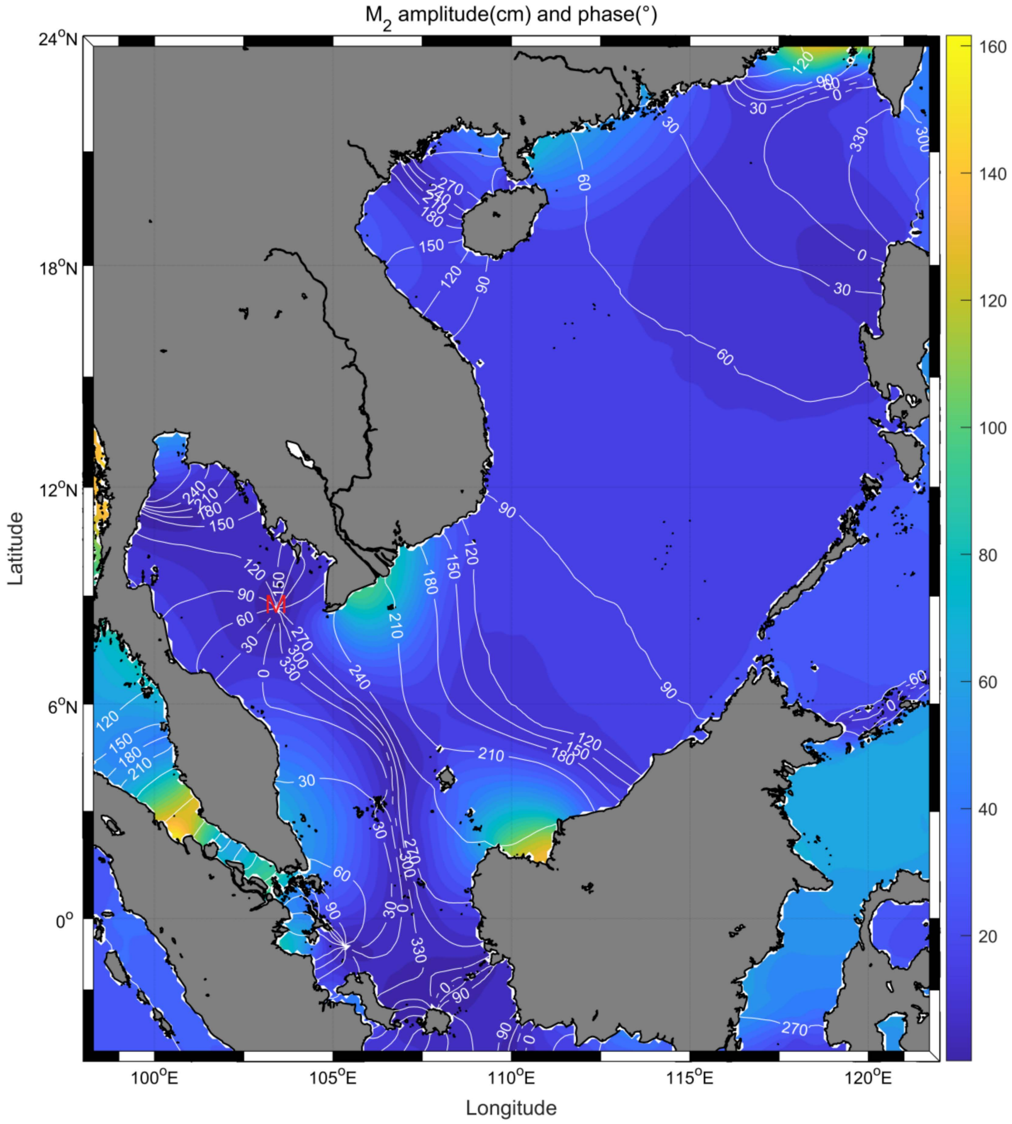

Figure 5. Same as Figure 1, but for the South China Sea.

Since the 1990s, with significant improvement in computing power, 3D tidal models are more common. Zhu and Fang [37] simulated the vertical structure of tidal currents in the Gulf of Tonkin with less computer time by combing 2D and 3D models. Guo and Yanagi [38] presented the vertical distribution of tidal currents in the BYECS for M_2, S_2, K_1, and O_1 constituents using a high-resolution three-dimensional numerical model (with 12.5 km resolution in the horizontal and 20 layers in the vertical). Wang et al. [39] computed M_2 tides and tidal currents in the BYECS by means of a new 3D semi-implicit numerical model and revealed that the current-amphidromic points at different layers were located at the same horizontal position. Based on the Regional Ocean Model System (ROMS [40]), Wu et al. [41] established a high-resolution ocean model with two-way nesting to simulate tides in the Zhoushan Archipelago waters and found that M_4 and M_6 tides mainly originate from advective nonlinearity, not bottom friction. Chu et al. [42] investigated tidal duration asymmetry induced by higher harmonics of the main constituents (M_4, MS_4, M_6, and MS_6) in the Zhoushan Archipelago using the Finite-Volume Coastal Ocean Model (FVCOM [43]). Their numerical results indicate that tides are flood-dominant in the Zhoushan Archipelago, and tidal asymmetry is enhanced from the open sea to coastal areas.

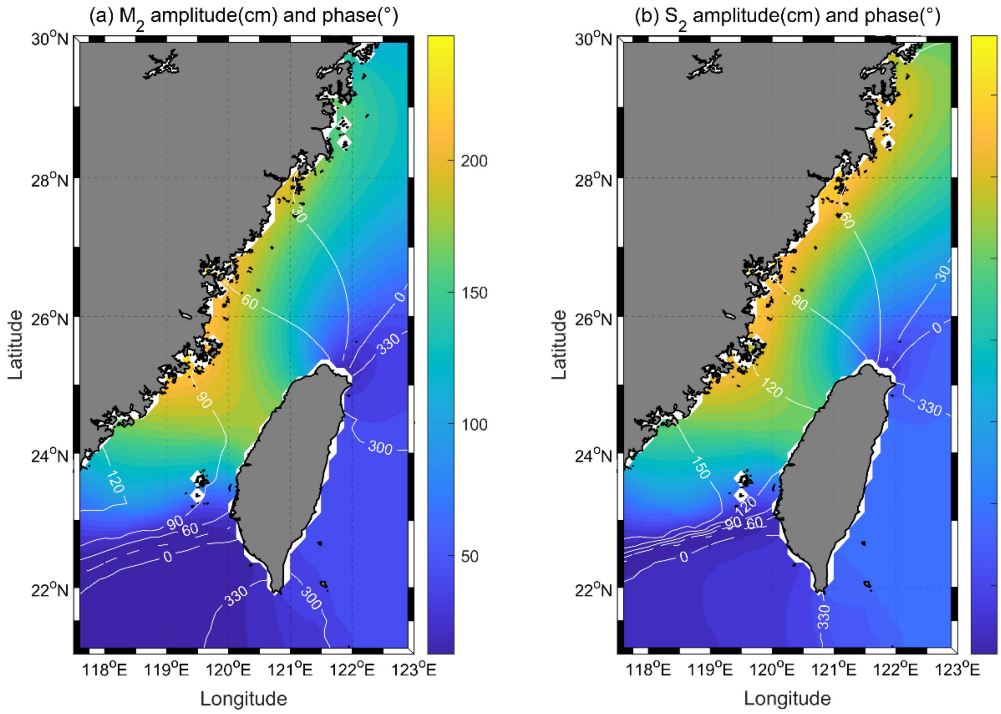

Figure 6. Cotidal charts for M_2 (**a**) and S_2 (**b**) tides in the Taiwan Strait.

3. Tidal Modeling with Data Assimilation

Since the launch of the TOPEX/Poseidon (T/P) satellite in 1992, satellite altimeter data have been assimilated into tidal models and significantly improved their accuracy. The flowchart for tidal modeling with the adjoint assimilation method is displayed in Figure 7. Han et al. [44] optimized the open boundary conditions (OBCs) by assimilating T/P observations to the adjoint tidal model for the East China Sea. He et al. [45] established a numerical adjoint model assimilating T/P data to investigate the shallow water constituents (M_4, MS_4, and M_6) in the BYS. Wu et al. [46] considered the equilibrium tides, optimized the OBCs, and assimilated T/P observations to the Princeton Ocean Model (POM [47]) for the South China Sea. Book et al. [48] assimilated moored ADCP, tide gauges, and altimeter records to a numerical model to optimize OBCs and obtained accurate barotropic tides in the Korea Strait. Jan et al. [49] used variational data assimilation to inverse the OBCs in a 3D ocean model for the Taiwan Strait. Lv and Zhang [14] derived spatially varying bottom friction coefficients (BFCs) in the BYECS via a 2D adjoint tidal model. To reduce the number of control variables and avoid the ill-posedness of the inverse problem, Lv and Zhang [14] used the independent point (IP) scheme, which meant that BFCs at the selected IPs were treated as independent parameters and that values at rest grid points were obtained by interpolation. Zu et al. [50] assimilated T/P data into a barotropic tide model for the eight main constituents in the South China Sea. They indicated that the response of tides in the South China Sea is closely related to the propagating directions of the tides from the Pacific, the wavelengths, the coastline, and the topography.

Zhang and Lu [51] simulated the 3D tidal currents in the BYS by assimilating satellite altimetry. Zhang et al. [52] studied the similarities and the differences between linear and nonlinear bottom friction parameterizations in the BYS using a 2D adjoint tidal model. Zhang and Wang [53] proposed a feature points method for inversion of periodic OBCs in the adjoint tidal model. Gao et al. [12] added a parameterized internal tide dissipation term in the adjoint tidal model to investigate tidal dynamics in the South China Sea and indicated that internal tide dissipation mainly occurred in the Luzon Strait and the central deep basin of the South China Sea. Pan et al. [2] proposed an improved IP scheme which used the Spline interpolation to replace the Cressman interpolation in the traditional IP scheme.

Practical experiments in the BYS indicated that the misfits between modeled results and observations were smaller when the improved IP scheme was applied [2]. The improved IP scheme has been used to optimize spatially varying BFCs in the Bohai Sea [15] and smoothly varying OBCs in the northern South China Sea [54]. Zheng et al. [55] developed a dynamically constrained interpolation methodology based on the adjoint method and successfully obtained an accurate M_2 cotidal chart in the BYECS. Qian et al. [56] assimilated multi-mission satellite observations to the adjoint tidal model and further improved the model's performance in the BYECS. Wang et al. [57,58] estimated spatially and temporally varying BFCs in the BYECS and indicated that BFCs are significantly related to the current speed and water depth.

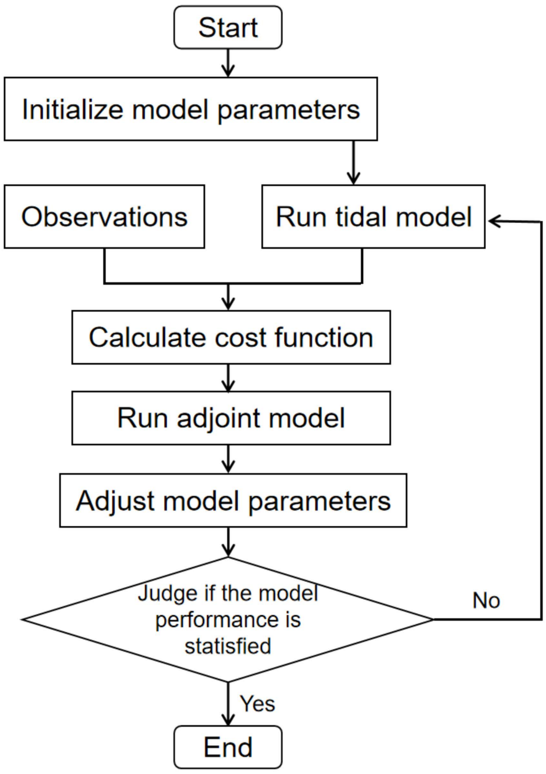

Figure 7. The flowchart for the adjoint tidal model.

Generally, most previous studies used the adjoint method to iteratively optimize the model parameters. Although the adjoint method is powerful, it is computationally expensive and technically demanding. Therefore, there exist a few studies using another assimilating method. Li et al. [59,60] used an artificial neural network to estimate optimal OBCs for regional tidal models. Moon et al. [61] applied a new method which used Green's function approach to optimize modal parameters and noticeably improved the accuracy of tidal simulation for the EAMS. Wei et al. [62] proposed an improved Nudging assimilation scheme and successfully applied it to simulate the M_2 constituent in the Northwest Pacific based on POM. Zhu et al. [63] assimilated coastal acoustic tomography observations to FVCOM via an Ensemble Kalman Filter scheme and studied the dynamics of tidal currents in the Jiaozhou Bay.

4. Changing Tides under Natural Variability and Human Activities

Due to non-astronomical perturbations such as river flow, sea ice, coastline, and water depth change related to human activities and sea level rise, tides show multiscale nonstationary changes [64,65]. Figure 8 displays the observed tides in the Yangtze river estuary (YRE) which are typical nonstationary tides. Tides are basically stationary and slightly influenced by river flow at Tianshenggang, located in the entrance of YRE. As tides propagate landward to Zhenjiang, they are significantly suppressed by river flow, especially in the flood season. Previous studies reviewed in Sections 2 and 3 all focus on modeling stationary tides which means that tidal amplitudes and phases are constant, thus, they ignore potential tidal evolution which is the main focus of recent tidal studies.

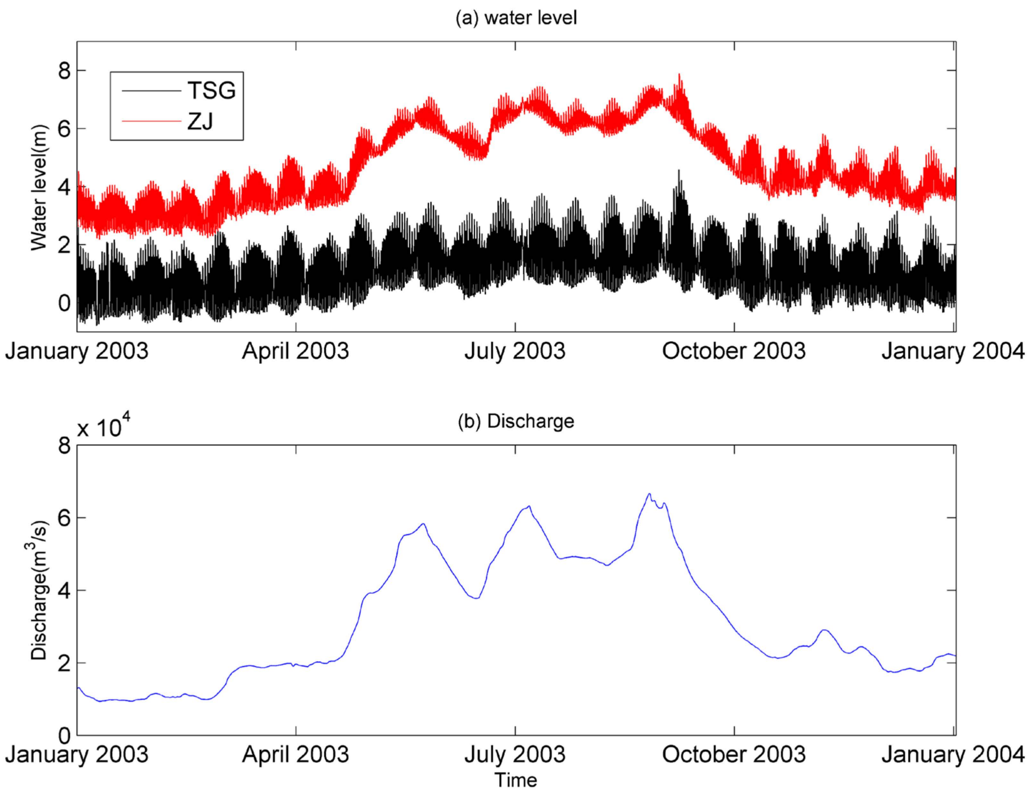

Figure 8. (**a**) Water levels at Tianshenggang (TSG) and Zhenjiang (ZJ). (**b**) Yangtze river discharge.

Pelling et al. [11] discussed the impact of rapid coastline changes to the M_2 tide in the Bohai Sea and found that M_2 amplitudes changed up to 20 cm in some parts. Lu et al. [66] explored tidal propagation, tidal distortion, and tidal damping in the YRE during the dry season using Delft-3D [67]. Zhang et al. [68,69] explored the seasonal variation of a tidal prism and energy in the YRE via the TELEMAC-2D model [70]. They indicated that tidal discharge showed a noticeable decreasing trend with the increase of river discharge rate while the tidal storage volume was insensitive to river discharge. Zhang et al. [71] quantified the tide–surge interaction in the east coast of the Leizhou Peninsula, South China Sea via POM and pointed out that the largest amplitudes of the tide–surge interaction can reach 1 m during typhoon events.

Zhang et al. [72] investigated seasonal interactions between tides and river flow in the YRE by Delft-3D and indicated that in the downstream reach of a tidal river, increasing discharge can reduce semi-diurnal amplitudes but amplify diurnal amplitudes. Zhu et al. [7] systematically explored the influences of changes in topography and coastline related to reclamation and coastal erosion on tidal systems, tidal currents, and tidal fluxes in the Bohai Sea from 1987 to 2016. They considered coastline changes in the Liaodong Bay that occurred in the 2010s, which was ignored by Pelling et al. [11]. It is found that the changes in M_2 amplitudes in the Bohai Sea are between -23.3 and 17.2 cm, while the variations in K_1 amplitudes range from -0.9 to 3.1 cm. Devlin et al. [73] found that seasonal tidal variability in the seas of Southeast Asia was correlated to the western North Pacific monsoon index. Via the model perturbation approach, Devlin et al. [73] indicated that seasonal tidal variability in the southern Gulf of Thailand and near Singapore was caused by the combined effects of geostrophic and wind-driven Ekman currents. Feng et al. [8] quantified the influence of satellite-based sea level trends on tidal changes in the Yellow Sea via FVCOM. They indicated that a significant decrease in tidal range laid in the northern shelf of the Yellow Sea, while the increase of tidal range was mainly located in the southern shelf.

Phan et al. [74] explored tidal wave propagation along the coast of the Mekong delta using Delft-3D, and their results indicate that wind monsoon climate can change tidal amplitudes along the Mekong deltaic coast about 2–3 cm. Zhang et al. [75] investigated the potential influence of sea ice on tides in the Bohai Sea via FVCOM. They found that sea ice almost did not alter M_2 phases but reduced M_2 amplitudes up to 1 cm. Guo et al. [76] employed Delft-3D to explore long-period tidal behaviors under changing river flow in the YRE. They indicated that estuaries act like a frequency filter, where long-period tidal waves damp at a smaller rate and propagate more upward than short-period tidal waves do. Wang et al. [13] discussed the seasonal tidal variability in the Bohai Sea via the Massachusetts Institute of Technology General Circulation Model (MITgcm [77]) and pointed out that seasonally the mean sea level, changing stratification, and vertical eddy should be responsible for seasonable tidal variability at Dalian. Zhao et al. [78] numerically investigated the potential influence of planned intense reclamation on the tides along the open coast in southeastern Zhejiang using the MIKE21 model. It was found that the tidal ranges were reduced, tidal directions were altered, and tidal refraction effects were weakened after land reclamation. Choi et al. [79,80] explored the tide–wave–surge interaction in the Yellow Sea via numerical models.

Feng and Feng [81] explored the influence of coastline changes and a rising sea level on tidal asymmetry along the coast of Jiangsu and found that the interactions between M_2/M_4 and $M_2/S_2/MS_4$ were most sensitive to coastline changes and contributed the largest part to tidal distortion. Using ROMS, Lin et al. [9] studied the tidal response to changes in coastline and water depth related to land reclamation and waterway dredging in the Pearl River Estuary (PRE). They indicated that coastline changes reduced the water area and volume in the PRE, which caused a decrease of 17.1% (11.3%) in the tidal prism during neap (spring) tides and induced a noticeable reduction of 19.0% in the tidal energy flux propagating into the PRE. Zhu et al. [82] explored decadal tidal changes caused by morphological and sedimentary evolution in the YRE via Delft-3D. They found that tidal damping increased in the mouth zone of the YRE since 1997, mainly because of stronger effective bottom roughness related to local engineering projects. They also indicated the dual influences of reduced sediment supply on tides: it strengthened tides in the South Branch through its effects on morphology but dampened tides via its effects on bottom friction.

5. Tidal Influence on the Ocean Environment

In Section 4, the impact of the changing ocean environment related to human activities and natural variability on tidal evolution is reviewed. In fact, tides can also change the ocean environment in turn. Numerous studies have indicated the important role of tides and tidal mixing on ocean circulation, the ocean ecosystem, and the global climate based on in situ and satellite observations [20,21,83]. It is found that satellite-derived sea surface temperature observations in the coastal waters of Hong Kong show significant spring-neap cycles which are vital indicators for tide-induced mixing [20]. Noticeable spring-neap signals which can change satellite-derived chlorophyll-a concentrations up to 12–33% are observed in the East China Sea and South China Sea [21]. Fortnightly cycles in satellite-observed sea surface temperature in the Indonesian seas show seasonal and interannual modulation that is related to the monsoon and El Niño Southern Oscillation (ENSO) [83].

There are also many studies which used numerical models to quantify the influence of tides on the marine environment. Lee et al. [84] investigated the influence of tides on the intermediate water in the East/Japan Sea by means of an eddy-resolving ocean model and indicated that tides enhanced vertical mixing and brought simulated water mass features closer to observations. Zhang et al. [85] quantified the tidal impact on the distribution of river discharge in the YRE by means of a 2D hydrodynamic model and found that tides can change the river discharge division by ~12% to 22% at Xuliujing bifurcation with river flows changing from 30,000 to 20,000 m^3s^{-1}. Ji and Zhang [86] explored the tidal influence on the evolution of river hydraulic geometry in the PRE via a 2D numerical model and indicated that the nonlinear tide–river interplay can create a water level setup which influences the discharge division at tidal bifurcations while the net tidal effect generally attenuates the inequality in the discharge division.

It is well-known that continental shelf circulation simulated by numerical models cannot display a reasonable vertical thermohaline structure in the absence of tides. Adding additional tidal forcing on the open boundary is a common method to include the influences of tidal mixing, however, this method is computationally expensive because the time scale of ocean tides is significantly smaller than that of ocean circulation. Therefore, Wei et al. [19] developed harmonic analyzed parameterization of tide-induced (HAT) mixing for ocean circulation models as an alternative to avoid running an independent tidal model. Differently from previous tidal mixing parameterization schemes which only consider spatial mixing coefficients, HAT additionally considers temporal changes of the tide-induced mixing coefficient caused by typical semi-diurnal and diurnal periods of tidal fluctuations. Figure 9 displays the results of a series of comparative numerical experiments in the BYECS with and without HAT via ROMS. Figure 9a is the result of a control experiment which adds explicit tidal forcing on the open boundary (Experiment 1), while Figure 9b shows the results without tidal forcing on the open boundary (Experiment 2). Figure 9c displays the results without tides but considering HAT (Experiment 3). It is clear that HAT successfully reproduces vertical temperature structures, similarly to the results obtained by directly adding tidal forcing on the open boundary, while HAT is computationally cheap.

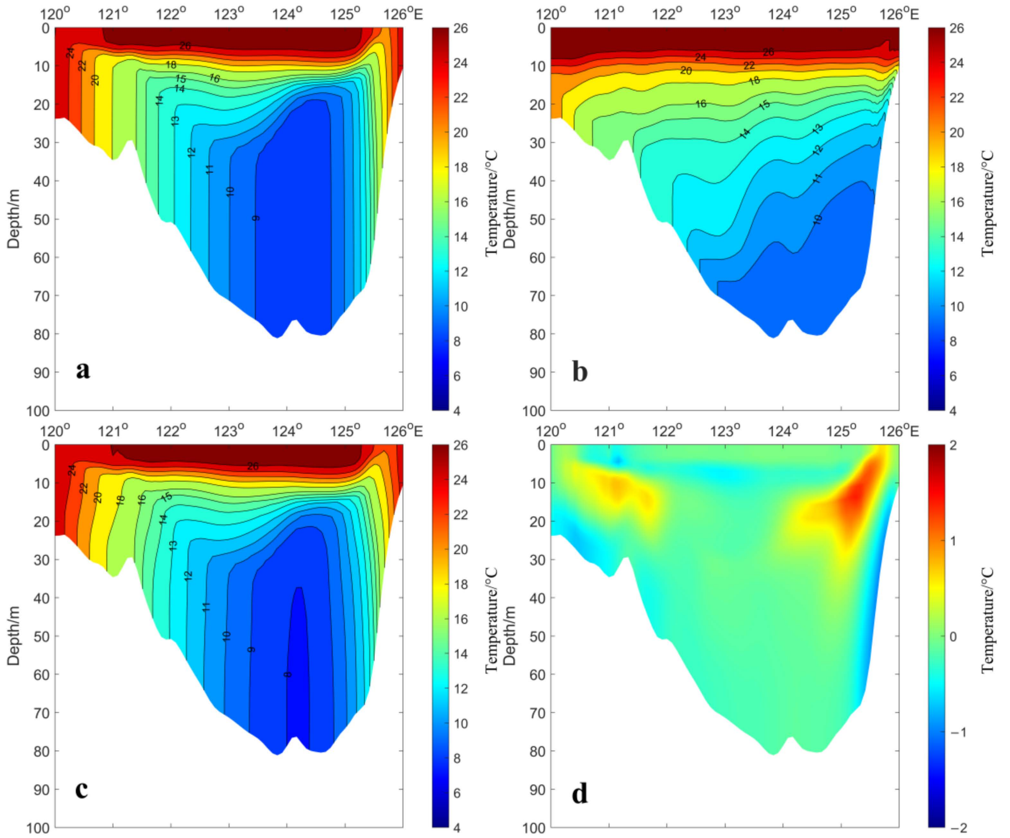

Figure 9. Modeled vertical temperature structures [19] along 35° N in August for Experiment 1 (**a**), Experiment 2 (**b**), and Experiment 3 (**c**). (**d**) Differences of modeled water temperature between Experiment 3 and Experiment 1.

6. Numerical Studies of Internal Tides

Internal tides are internal waves with tidal frequencies which are generated in the stratified ocean when barotropic tides interplay with topography and play a vital role in deep ocean mixing and energy dissipation of barotropic tides [17]. Internal tides are ubiquitous in East Asian marginal seas and especially significant in the South China Sea. Thus, the South China Sea is a hot spot for the research of internal tides. Yuan et al. [87] developed a three-layer tidal model to investigate the generation of internal tides in the northeastern South China Sea. Their results showed that M_2 internal tides were mainly generated in the shelf break south of the Taiwan shoal, while K_1 internal tides were mainly generated in the shelf break southeast of the Yitong shoal. Fang et al. [88] developed a layered 3D tidal model whose surface can simultaneously simulate barotropic and baroclinic tides, and successfully simulated internal tides in the northwestern South China Sea. Combined with the observational feature of internal tides in the sea area around the Nansha Islands, Cai et al. [89] used a two-layer ocean model to investigate the generation of internal tides in the shelf break. It was found that internal tidal amplitudes can be influenced by the source depth of barotropic tides, nonlinear effects, and wind stress.

Jan et al. [16] investigated the spatial and seasonal variability of internal tides in the Luzon Strait using POM and indicated that there was no noticeable seasonal variation of baroclinic tidal energy, but the propagation speed of internal tide waves was about 10% slower in the winter than in the summer. Miao et al. [90] developed a three-dimensional isopycnic-coordinate ocean model for internal tides and applied it to the South China Sea. They found that the K_1 internal tides generated in the Luzon Strait propagated away in two distinct branches: one branch propagated southwestward into the South China Sea with a beam width of ~250 km; the other branch propagated eastward into the Pacific with a beam width of ~450 km. Wang et al. [91] explored the generation of internal tides in the Luzon Strait via POM and found that the diurnal modulation of semi-diurnal internal tides was induced by the interplay between the linear internal waves and barotropic diurnal tidal currents. Wu et al. [92] discussed the seasonal variability of M_2 and K_1 internal tides in the northern South China Sea using MITgcm. Their numerical results indicated that ocean mixing caused by internal tides in the summer was weaker than those in the winter in the northern South China Sea.

Guo et al. [93] explored how the seasonal variations of ocean stratification influenced the generation of internal tides in the Luzon Strait. They indicated that the seasonal changes of ocean stratification influenced the wavelength of internal tides and the interference of local topography within internal tides, which finally altered baroclinic energy conversion in the Luzon Strait. Based on mooring observations, Yan et al. [18] found that internal tides in the northwestern South China Sea were strong in the summer but negligible in the winter. Their numerical results indicated that the seasonal changing ocean stratification controlled the seasonality of internal tides. In the summer, due to strong stratified layers, baroclinic tides can be generated locally or remotely and easily propagated across the shelf, while in the winter, internal tides dissipate at the shelf break because of the disappearance of ocean stratification caused by uniformly vertical mixing. Guo et al. [94] employed the Coastal and Regional Ocean COmmunity (CROCO) model to investigate the impact of internal tides originating from the Luzon Strait on the local generation of internal tides on the continental slope in the South China Sea. It was found that remote internal tides can noticeably change the phases and amplitudes of the pressure perturbation on the continental shelf, thus, influence the local generation of internal tides.

Wang et al. [95] explored the reflection of the K_1 internal tides at the continental shelf break in the northern South China Sea via MITgcm. K_1 internal tides originated from the Luzon Strait propagate westward into the northern South China Sea with energy of 3.54 GW and then, 0.31 GW of energy are reflected by the shelf break. There exist two reflected beams caused by the complicated bottom topography. The southeast one is dominant and can spread across the deep basin of the South China Sea, consistent with satellite altimeter observations. The other one propagating eastward to the Luzon Strait is weak and absent in altimeter observations due to its low intensity. Li et al. [96] discussed the modulation of internal tides caused by turbulent mixing in the South China Sea using MITgcm and indicated that turbulent mixing altered horizontal density in the South China Sea and then increased the incoherence of internal tides.

In recent years, the internal tides in the Yellow Sea and the East/Japan Sea receive more and more attention. Jiang and Lv [97] studied the basic feature of M_2, S_2, K_1, and O_1 internal tides in the BYECS via a 3D layered tidal model. They found that internal tides are mainly generated in the Okinawa Trough and are stronger in the winter than in the summer. Jeon et al. [98] used an eddy-resolving high-resolution ocean model to investigate the seasonal variability of semi-diurnal internal tides in the East/Japan Sea. Their results indicated that due to the seasonality in ocean stratification near the south-western East/Japan Sea, baroclinic energy conversion varied seasonally with minima in March (ranging from 0.11 to 0.16 GW) and maxima in September (ranging from 0.48 to 0.52 GW). The seasonal and spatial variations of M_2 internal tides in the Yellow Sea are studied by Liu et al. [17] via ROMS. They found that seasonal ocean stratification, induced by the East Asian monsoon, seasonal ocean circulation, and Yangtze river flow, controls the seasonal variations of the generation, propagation, and dissipation of M_2 internal tides in the Yellow Sea. Lin et al. [99] investigated M_2 internal tides in the northern Yellow Sea in the summer via ROMS and moored current observations. They indicated that internal tides are mainly generated in the shelf break regions near the Korean Peninsula with a restricted regional propagation.

7. Summary and Prospect

Tides play an important role in numerous economic sections such as coastal engineering, maritime logistics, and fishery [1]. Significant progresses in tidal dynamics in the EAMS have been made over the past few decades mainly due to ample water-level observations (especially satellite altimeter data) and improved numerical models with data assimilation [3–10]. The basic characteristics of barotropic tides in the EAMS are very clear, and the accuracy of ocean tide models is generally satisfactory. The focus of tidal research is gradually changing from stationary tides to nonstationary tides (such as river tides, internal tides) which show significant non-astronomical variations caused by natural variability and human interference. It is found that tides show multi-time scale variations (from seasonal to multi-decadal), which are not fully understood [100]. There are only few publicly accessible long-term (more than 20 years) tide gauges in the EAMS, which is not conducive to our understanding on secular tidal evolution. The impact of tides and tidal mixing on the ocean environment and climate is a potential hotspot. Tidal influences on the ocean ecosystem and climate modes have been reported based on observations, but detailed physical mechanisms are still unclear and can be further explored by means of numerical models. Furthermore, the nascent artificial intelligence methods, such as deep learning, provide an unprecedented opportunity to help tidal researchers analyze water-level data. The combination of artificial intelligence and ocean tidal models is another potential hotspot.

Author Contributions: Conceptualization, Z.W. and H.P.; writing—original draft preparation, Z.W. and H.P.; writing—review and editing, Z.W., H.P., T.X., Y.W., J.W.; visualization, H.P.; supervision, Z.W. All authors have read and agreed to the published version of the manuscript.

Funding: This study is jointly supported by National Natural Science Foundation of China (42076024), the Qingdao postdoctoral application research project (QDBSH202108) and China Postdoctoral Science Foundation (2022M713677).

Institutional Review Board Statement: Not applicable.

Informed Consent Statement: Not applicable.

Data Availability Statement: The reader can ask for all the related data from the corresponding author (weizx@fio.org.cn).

Acknowledgments: We are very grateful to Byung Ho Choi for his selfless help to us. All of us share the good fortune to have had him as an extraordinary friend, from which we all benefited.

Conflicts of Interest: The authors declare no conflict of interest.

References

1. Gan, M.; Pan, H.; Chen, Y.; Pan, S. Application of the Variational Mode Decomposition (VMD) Method to River Tides. *Estuar. Coast. Shelf Sci.* **2021**, *261*, 107570. [CrossRef]
2. Pan, H.; Guo, Z.; Lv, X. Inversion of Tidal Open Boundary Conditions of the M_2 Constituent in the Bohai and Yellow Seas. *J. Atmos. Ocean. Technol.* **2017**, *34*, 1661–1672. [CrossRef]
3. Choi, B.H.; Ko, J.S. Modeling of tides in the East Asian Marginal Seas. *J. Korean Soc. Coast. Ocean Eng.* **1994**, *6*, 94–108.
4. Choi, B.H. *Tides in the East Asian Marginal Seas*; Hanrimwon Publishing Co.: Seoul, Korea, 2015; pp. 1–15.
5. Shen, Y. Numerical Computation of Tides in the East China Sea. *J. Shandong Coll. Oceanol.* **1980**, *10*, 26–35.
6. Choi, B.H. Development of fine-grid numerical tidal models of the Yellow Sea and the East China Sea. *J. Korean Soc. Coast. Ocean Eng.* **1990**, *2*, 231–234. [CrossRef]
7. Zhu, L.; Hu, R.; Zhu, H.; Jiang, S.; Xu, Y.; Wang, N. Modeling Studies of Tidal Dynamics and the Associated Responses to Coastline Changes in the Bohai Sea, China. *Ocean Dyn.* **2018**, *68*, 1625–1648. [CrossRef]
8. Feng, X.; Feng, H.; Li, H.; Zhang, F.; Feng, W.; Zhang, W.; Yuan, J. Tidal Responses to Future Sea Level Trends on the Yellow Sea Shelf. *J. Geophys. Res. Ocean.* **2019**, *124*, 7285–7306. [CrossRef]
9. Lin, S.; Liu, G.; Niu, J.; Wei, X.; Cai, S. Responses of Hydrodynamics to Changes in Shoreline and Bathymetry in the Pearl River Estuary, China. *Cont. Shelf Res.* **2021**, *229*, 104556. [CrossRef]
10. An, H.S. A Numerical Experiment of the M_2 Tide in the Yellow Sea. *J. Oceanogr. Soc. Jpn.* **1977**, *33*, 103–110. [CrossRef]
11. Pelling, H.E.; Uehara, K.; Green, J.A.M. The Impact of Rapid Coastline Changes and Sea Level Rise on the Tides in the Bohai Sea, China. *J. Geophys. Res. Ocean.* **2013**, *118*, 3462–3472. [CrossRef]
12. Gao, X.; Wei, Z.; Lv, X.; Wang, Y.; Fang, G. Numerical Study of Tidal Dynamics in the South China Sea with Adjoint Method. *Ocean Model.* **2015**, *92*, 101–114. [CrossRef]
13. Wang, D.; Pan, H.; Jin, G.; Lv, X. Seasonal Variation of the Principal Tidal Constituents in the Bohai Sea. *Ocean Sci.* **2020**, *16*, 1–14. [CrossRef]
14. Lv, X.; Zhang, J. Numerical Study on Spatially Varying Bottom Friction Coefficient of a 2D Tidal Model with Adjoint Method. *Cont. Shelf Res.* **2006**, *26*, 1905–1923. [CrossRef]
15. Guo, Z.; Pan, H.; Fan, W.; Lv, X. Application of Surface Spline Interpolation in Inversion of Bottom Friction Coefficients. *J. Atmos. Ocean. Technol.* **2017**, *34*, 2021–2028. [CrossRef]
16. Jan, S.; Lien, R.C.; Ting, C.H. Numerical Study of Baroclinic Tides in Luzon Strait. *J. Oceanogr.* **2008**, *64*, 789–802. [CrossRef]
17. Liu, K.; Sun, J.; Guo, C.; Yang, Y.; Yu, W.; Wei, Z. Seasonal and Spatial Variations of the M_2 Internal Tide in the Yellow Sea. *J. Geophys. Res. Ocean.* **2019**, *124*, 1115–1138. [CrossRef]
18. Yan, T.; Qi, Y.; Jing, Z.; Cai, S. Seasonal and Spatial Features of Barotropic and Baroclinic Tides in the Northwestern South China Sea. *J. Geophys. Res. Ocean.* **2020**, *125*, e2018JC014860. [CrossRef]
19. Wei, Z.; Sun, J.; Teng, F.; Xu, T.; Wang, Y.; Xu, X.; Fang, G. A Harmonic Analyzed Parameterization of Tide-Induced Mixing for Ocean Models. *Acta Oceanol. Sin.* **2018**, *37*, 1–7. [CrossRef]
20. Susanto, R.D.; Pan, J.; Devlin, A.T. Tidal Mixing Signatures in the Hong Kong Coastal Waters from Satellite-Derived Sea Surface Temperature. *Remote Sens.* **2018**, *11*, 5. [CrossRef]
21. Xing, Q.; Yu, H.; Yu, H.; Wang, H.; Ito, S.I.; Yuan, C. Evaluating the Spring-Neap Tidal Effects on Chlorophyll-a Variations Based on the Geostationary Satellite. *Front. Mar. Sci.* **2021**, *8*, 758538. [CrossRef]
22. Fang, G. A Two-Dimensional Numerical Model for Tidal, Motion in the Taiwan Strait. *Mar. Geophys. Res.* **1984**, *7*, 267–276. [CrossRef]
23. Fang, G.; Yang, J. A Two-Dimensional Numerical Model of the Tidal Motions in the Bohai Sea. *Chin. J. Oceanol. Limnol.* **1985**, *3*, 135–152. [CrossRef]
24. Fang, G. A Finite Difference-Least Square Technique for Solving Tidal Wave Equations with Specific Application to the Modeling of M_2 Tide in the Huanghai Sea. *Sci. Sin.* **1985**, *28*, 1110–1120.
25. Fang, G. Tide and Tidal Current Charts for the Marginal Seas Adjacent to China. *Chin. J. Oceanol. Limnol.* **1986**, *4*, 1–16. [CrossRef]
26. Fang, G.; Yang, J. Modeling and Prediction of Tidal Currents in the Korea Strait. *Prog. Oceanogr.* **1988**, *21*, 307–318. [CrossRef]
27. Odamaki, M. Co-Oscillating and Independent Tides of the Japan Sea. *J. Oceanogr. Soc. Jpn.* **1989**, *45*, 217–232. [CrossRef]
28. Cao, D.; Fang, G. A Numerical Model of the Tides and Tidal Currents in Beibu Bay. *Oceanol. Limnol. Sin.* **1990**, *21*, 105–113.
29. Choi, B.H.; Fang, G. A Review of Tidal Models for the East China and Yellow Seas. *J. Korean Soc. Coast. Ocean Eng.* **1993**, *5*, 151–171.
30. Zhao, B.; Fang, G.; Cao, D. Characteristics of Tidal Residual Currents and Their Relations with Coastal Current Transports in the Bohai Sea, Yellow Sea and East China Sea. *Stud. Mar. Sin.* **1995**, *36*, 1–11.
31. Fang, G.; Kwok, Y.K.; Yu, K.; Zhu, Y. Numerical Simulation of Principal Tidal Constituents in the South China Sea, Gulf of Tonkin and Gulf of Thailand. *Cont. Shelf Res.* **1999**, *19*, 845–869. [CrossRef]
32. Hart-Davis, M.G.; Piccioni, G.; Dettmering, D.; Schwatke, C.; Passaro, M.; Seitz, F. EOT20: A Global Ocean Tide Model from Multi-Mission Satellite Altimetry. *Earth Syst. Sci. Data* **2021**, *13*, 3869–3884. [CrossRef]

33. Lin, M.C.; Juang, W.J.; Tsay, T.K. Anomalous Amplifications of Semidiurnal Tides along the Western Coast of Taiwan. *Ocean Eng.* **2001**, *28*, 1171–1198. [CrossRef]
34. Jan, S.; Chern, C.S.; Wang, J. Transition of Tidal Waves from the East to South China Seas over the Taiwan Strait: Influence of the Abrupt Step in the Topography. *J. Oceanogr.* **2002**, *58*, 837–850. [CrossRef]
35. Teng, F.; Fang, G.; Xu, X. Effects of Internal Tidal Dissipation and Self-Attraction and Loading on Semidiurnal Tides in the Bohai Sea, Yellow Sea and East China Sea: A Numerical Study. *Chin. J. Oceanol. Limnol.* **2017**, *35*, 987–1001. [CrossRef]
36. Zhang, Q.; Su, M.; Yao, P.; Chen, Y.; Stive, M.J.F.; Wang, Z.B. Dynamics of a Tidal Current System in a Marginal Sea: A Case Study of the Yellow Sea, China. *Front. Mar. Sci.* **2020**, *7*, 596388. [CrossRef]
37. Zhu, Y.; Fang, G. A Combined Two-and-Three Dimensional Numerical Hydrodynamical Model with Application to Simulation of Tidal Motions in the Beibuwan Gulf (Gulf of Tonkin). *Oceanol. Limnol. Sin.* **1993**, *24*, 117–125.
38. Guo, X.; Yanagi, T. Three-Dimensional Structure of Tidal Current in the East China Sea and the Yellow Sea. *J. Oceanogr.* **1998**, *54*, 651–668. [CrossRef]
39. Wang, K.; Fang, G.; Feng, S. A 3-D numerical simulation of M2 tides and tidal currents in the Bohai Sea, the Huanghai Sea and the East China Sea. *ACTA Oceanol. Sin.* **1999**, *21*, 1–13.
40. Shchepetkin, A.F.; McWilliams, J.C. The regional oceanic modeling system (ROMS): A split-explicit, free-surface, topography-following-coordinate oceanic model. *Ocean Model.* **2015**, *9*, 347–404. [CrossRef]
41. Wu, R.; Jiang, Z.; Li, C. Revisiting the Tidal Dynamics in the Complex Zhoushan Archipelago Waters: A Numerical Experiment. *Ocean Model.* **2018**, *132*, 139–156. [CrossRef]
42. Chu, D.; Niu, H.; Wang, Y.P.; Cao, A.; Li, L.; Du, Y.; Zhang, J. Numerical Study on Tidal Duration Asymmetry and Shallow-Water Tides within Multiple Islands: An Example of the Zhoushan Archipelago. *Estuar. Coast. Shelf Sci.* **2021**, *262*, 107576. [CrossRef]
43. Chen, C.; Liu, H.; Beardsley, R.C. An unstructured grid, finite-volume, threedimensional, primitive equations ocean model: Application to coastal ocean and estuaries. *J. Atmos. Ocean. Technol.* **2003**, *20*, 159–186. [CrossRef]
44. Han, G.; Fang, G.; Ma, J.; Liu, K.; Li, D. Optimizing Open Boundary Conditions of Nonlinear Tidal Model Using Adjoint Method. *ACTA Oceanol. Sin.* **2001**, *23*, 25–31.
45. He, Y.; Lu, X.; Qiu, Z.; Zhao, J. Shallow Water Tidal Constituents in the Bohai Sea and the Yellow Sea from a Numerical Adjoint Model with TOPEX/POSEIDON Altimeter Data. *Cont. Shelf Res.* **2004**, *24*, 1521–1529. [CrossRef]
46. Wu, Z.; Tian, J.; Zhao, Q. 3-D Numerical Simulation of the South China Sea Tidal Waves with Assimilation Method. *J. Hydrodyn.* **2004**, *19*, 501–506. [CrossRef]
47. Blumberg, A.F.; Mellor, G.F. Three-Dimensional Coastal Ocean Models. *Coast. Estuar. Stud.* **1987**, *4*, 1–16.
48. Book, J.W.; Pistek, P.; Perkins, H.; Thompson, K.R.; Teague, W.J.; Jacobs, G.A.; Suk, M.S.; Chang, K.I.; Lee, J.C.; Choi, B.H. Data Assimilation Modeling of the Barotropic Tides in the Korea/Tsushima Strait. *J. Oceanogr.* **2004**, *60*, 977–993. [CrossRef]
49. Jan, S.; Wang, Y.H.; Wang, D.P.; Chao, S.Y. Incremental Inference of Boundary Forcing for a Three-Dimensional Tidal Model: Tides in the Taiwan Strait. *Cont. Shelf Res.* **2004**, *24*, 337–351. [CrossRef]
50. Zu, T.; Gan, J.; Erofeeva, S.Y. Numerical Study of the Tide and Tidal Dynamics in the South China Sea. *Deep Sea Res. Part I Oceanogr. Res. Pap.* **2008**, *55*, 137–154. [CrossRef]
51. Zhang, J.; Lu, X. Inversion of Three-Dimensional Tidal Currents in Marginal Seas by Assimilating Satellite Altimetry. *Comput. Methods Appl. Mech. Eng.* **2010**, *199*, 3125–3136. [CrossRef]
52. Zhang, J.; Lu, X.; Wang, P.; Wang, Y.P. Study on Linear and Nonlinear Bottom Friction Parameterizations for Regional Tidal Models Using Data Assimilation. *Cont. Shelf Res.* **2011**, *31*, 555–573. [CrossRef]
53. Zhang, J.; Wang, Y.P. A Method for Inversion of Periodic Open Boundary Conditions in Two-Dimensional Tidal Models. *Comput. Methods Appl. Mech. Eng.* **2014**, *275*, 20–38. [CrossRef]
54. Jiang, D.; Chen, H.; Jin, G.; Lv, X. Estimating Smoothly Varying Open Boundary Conditions for a 3D Internal Tidal Model with an Improved Independent Point Scheme. *J. Atmos. Ocean. Technol.* **2018**, *35*, 1299–1311. [CrossRef]
55. Zheng, J.; Mao, X.; Lv, X.; Jiang, W. The M2 Cotidal Chart in the Bohai, Yellow, and East China Seas from Dynamically Constrained Interpolation. *J. Atmos. Ocean. Technol.* **2020**, *37*, 1219–1229. [CrossRef]
56. Qian, S.; Wang, D.; Zhang, J.; Li, C. Adjoint Estimation and Interpretation of Spatially Varying Bottom Friction Coefficients of the M2 Tide for a Tidal Model in the Bohai, Yellow and East China Seas with Multi-Mission Satellite Observations. *Ocean Model.* **2021**, *161*, 101783. [CrossRef]
57. Wang, D.; Zhang, J.; Wang, Y.P. Estimation of Bottom Friction Coefficient in Multi-Constituent Tidal Models Using the Adjoint Method: Temporal Variations and Spatial Distributions. *J. Geophys. Res. Ocean.* **2021**, *126*, 1–20. [CrossRef]
58. Wang, D.; Zhang, J.; Mu, L. A Feature Point Scheme for Improving Estimation of the Temporally Varying Bottom Friction Coefficient in Tidal Models Using Adjoint Method. *Ocean Eng.* **2021**, *220*, 108481. [CrossRef]
59. Li, M.; Liang, S.; Sun, Z. Optimization Inversion Method for Tidal Model under Open Boundary Condition: A Case Study of K_1 Constituent Amplitude. *Adv. Water Sci.* **2009**, *20*, 129–134. [CrossRef]
60. Li, M.; Si, Q.; Liang, S.; Sun, Z.; You, X. Applied Data Driven Model for Current Field Calibration under the Condition of Open Boundary. *J. Water Resour. Water Eng.* **2011**, *22*, 7–10.
61. Moon, J.H.; Hirose, N.; Morimoto, A. Green's Function Approach for Calibrating Tides in a Circulation Model for the East Asian Marginal Seas. *J. Oceanogr.* **2012**, *68*, 345–354. [CrossRef]

62. Wei, Z.; Wang, Y.; Gao, X.; Fang, G. Improved Nudging Assimilation Schemes and Their Applications in Simulating M_2 Tide in the Northwest Pacific. *Adv. Mar. Sci.* **2015**, *33*, 431–438.
63. Zhu, Z.N.; Zhu, X.H.; Zhang, C.; Chen, M.; Wang, M.; Dong, M.; Liu, W.; Zheng, H.; Kaneko, A. Dynamics of Tidal and Residual Currents Based on Coastal Acoustic Tomography Assimilated Data Obtained in Jiaozhou Bay, China. *J. Geophys. Res. Ocean.* **2021**, *126*, 1–26. [CrossRef]
64. Pan, H.; Lv, X.; Wang, Y.; Matte, P.; Chen, H.; Jin, G. Exploration of Tidal-Fluvial Interaction in the Columbia River Estuary Using S_TIDE. *J. Geophys. Res. Ocean.* **2018**, *123*, 6598–6619. [CrossRef]
65. Pan, H.; Lv, X. Is There a Quasi 60-Year Oscillation in Global Tides? *Cont. Shelf Res.* **2021**, *222*, 104433. [CrossRef]
66. Lu, S.; Tong, C.; Lee, D.Y.; Zheng, J.; Shen, J.; Zhang, W.; Yan, Y. Propagation of Tidal Waves up in Yangtze Estuary during the Dry Season. *J. Geophys. Res. Ocean.* **2015**, *120*, 6445–6473. [CrossRef]
67. WL Delft Hydraulics. *User Manual Delft3D-FLOW*; WL Delft Hydraulics: Delft, The Netherlands, 1999.
68. Zhang, M.; Townend, I.; Zhou, Y.; Cai, H. Seasonal Variation of River and Tide Energy in the Yangtze Estuary, China. *Earth Surf. Process. Landforms* **2015**, *41*, 98–116. [CrossRef]
69. Zhang, M.; Townend, I.H.; Cai, H.; Zhou, Y. Seasonal Variation of Tidal Prism and Energy in the Changjiang River Estuary: A Numerical Study. *Chin. J. Oceanol. Limnol.* **2016**, *34*, 219–230. [CrossRef]
70. Hervouet, J.M. *Hydrodynamics of Free Surface Flows: Modelling with the Finite Element Method*; John Wiley & Sons: New York, NY, USA, 2007.
71. Zhang, H.; Cheng, W.; Qiu, X.; Feng, X.; Gong, W. Tide-Surge Interaction along the East Coast of the Leizhou Peninsula, South China Sea. *Cont. Shelf Res.* **2017**, *142*, 32–49. [CrossRef]
72. Zhang, F.; Sun, J.; Lin, B.; Huang, G. Seasonal Hydrodynamic Interactions between Tidal Waves and River Flows in the Yangtze Estuary. *J. Mar. Syst.* **2018**, *186*, 17–28. [CrossRef]
73. Devlin, A.T.; Zaron, E.D.; Jay, D.A.; Talke, S.A.; Pan, J. Seasonality of Tides in Southeast Asian Waters. *J. Phys. Oceanogr.* **2018**, *48*, 1169–1190. [CrossRef]
74. Phan, H.M.; Ye, Q.; Reniers, A.J.H.M.; Stive, M.J.F. Tidal Wave Propagation along The Mekong Deltaic Coast. *Estuar. Coast. Shelf Sci.* **2019**, *220*, 73–98. [CrossRef]
75. Zhang, N.; Wang, J.; Wu, Y.; Wang, K.H.; Zhang, Q.; Wu, S.; You, Z.J.; Ma, Y. A Modelling Study of Ice Effect on Tidal Damping in the Bohai Sea. *Ocean Eng.* **2019**, *173*, 748–760. [CrossRef]
76. Guo, L.; Zhu, C.; Wu, X.; Wan, Y.; Jay, D.A.; Townend, I.; Wang, Z.B.; He, Q. Strong Inland Propagation of Low-Frequency Long Waves in River Estuaries. *Geophys. Res. Lett.* **2020**, *47*, 1–11. [CrossRef]
77. Marshall, J.; Adcroft, A.; Hill, C.; Perelman, L.; Heisey, C. A finite-volume, incompressible Navier Stokes model for studies of the ocean on parallel computers. *J. Geophys. Res. Ocean.* **1997**, *102*, 5753–5766. [CrossRef]
78. Zhao, X.; Sun, Z.; Huang, S.; Liu, X.; Hu, Z. Numerical Study of the Tidal Refraction Effect on the Open Coast in Southeastern Zhejiang. *J. Oceanogr.* **2020**, *76*, 43–56. [CrossRef]
79. Choi, B.H.; Eum, H.M.; Woo, S.B. Modeling of coupled tide-wave-surge process in the Yellow Sea. *Ocean Eng.* **2003**, *30*, 739–759. [CrossRef]
80. Choi, B.H.; Eum, H.M.; Woo, S.B. A synchronously coupled tide-wave-surge model of the Yellow Sea. *Coast. Eng.* **2003**, *47*, 381–398. [CrossRef]
81. Feng, X.; Feng, H. On the Role of Anthropogenic Activity and Sea-Level-Rise in Tidal Distortion on the Open Coast of the Yellow Sea Shelf. *J. Geophys. Res. Ocean.* **2021**, *126*, 1–27. [CrossRef]
82. Zhu, C.; Guo, L.; van Maren, D.S.; Wang, Z.B.; He, Q. Exploration of Decadal Tidal Evolution in Response to Morphological and Sedimentary Changes in the Yangtze Estuary. *J. Geophys. Res. Ocean.* **2021**, *126*, 1–19. [CrossRef]
83. Susanto, R.D.; Ray, R.D. Seasonal and Interannual Variability of Tidal Mixing Signatures in Indonesian Seas from High-Resolution Sea Surface Temperature. *Remote Sens.* **2022**, *14*, 1934. [CrossRef]
84. Lee, H.J.; Park, J.H.; Wimbush, M.; Jung, K.T.; Jang, C.J.; Cho, Y.K.; Seo, Y.K.; Nam, J.H. Tidal Effects on Intermediate Waters: A Case Study in the East/Japan Sea. *J. Phys. Oceanogr.* **2011**, *41*, 234–240. [CrossRef]
85. Zhang, W.; Feng, H.; Hoitink, A.J.F.; Zhu, Y.; Gong, F.; Zheng, J. Tidal Impacts on the Subtidal Flow Division at the Main Bifurcation in the Yangtze River Delta. *Estuar. Coast. Shelf Sci.* **2017**, *196*, 301–314. [CrossRef]
86. Ji, X.; Zhang, W. Tidal Impacts on Downstream Hydraulic Geometry of a Tide-Influenced Delta. *Ocean Dyn.* **2020**, *70*, 1239–1252. [CrossRef]
87. Yuan, S.; Xu, X.; Deng, J.; Qiu, Z. A Numerical Study on Internal Tides in the Northeast of South China Sea. *Trop. Oceanol.* **1995**, *14*, 15–23.
88. Fang, G.; Li, H.; Du, T. A Layered 3-D Numerical Ocean Model for Simulation of Internal Tides. *Stud. Mar. Sin.* **1997**, *38*, 1–15.
89. Cai, S.; Huang, Q.; Qiu, Z.; Mai, B. A Numerical Study on Dynamic Mechanism of Internal Tide. *Trop. Oceanol.* **2000**, *19*, 27–32.
90. Miao, C.; Chen, H.; Lv, X. An Isopycnic-Coordinate Internal Tide Model and Its Application to the South China Sea. *Chin. J. Oceanol. Limnol.* **2011**, *29*, 1339–1356. [CrossRef]
91. Wang, D.P. Diurnal Modulation of Semidiurnal Internal Tides in Luzon Strait. *Ocean Model.* **2012**, *59–60*, 1–10. [CrossRef]
92. Wu, L.; Miao, C.; Zhao, W. Patterns of K_1 and M_2 Internal Tides and Their Seasonal Variations in the Northern South China Sea. *J. Oceanogr.* **2013**, *69*, 481–494. [CrossRef]

93. Guo, Z.; Cao, A.; Lv, X.; Song, J. Impacts of Stratification Variation on the M2 Internal Tide Generation in Luzon Strait. *Atmos.-Ocean* **2020**, *58*, 206–218. [CrossRef]
94. Guo, Z.; Cao, A.; Wang, S. Influence of Remote Internal Tides on the Locally Generated Internal Tides upon the Continental Slope in the South China Sea. *J. Mar. Sci. Eng.* **2021**, *9*, 1268. [CrossRef]
95. Wang, S.; Cao, A.; Li, Q.; Chen, X. Reflection of K_1 Internal Tides at the Continental Slope in the Northern South China Sea. *J. Geophys. Res. Ocean.* **2021**, *126*, 1–20. [CrossRef]
96. Li, B.; Du, L.; Peng, S.; Yuan, Y.; Meng, X.; Lv, X. Modulation of Internal Tides by Turbulent Mixing in the South China Sea. *Front. Mar. Sci.* **2021**, *8*, 772979. [CrossRef]
97. Jiang, B.; Lv, X. Three-Dimensional Numerical Simulation of Internal Tides in the Bohai Sea, the Yellow Sea and the East China Sea. *Trans. Oceanol. Limnol.* **2007**, *1*, 30–37.
98. Jeon, C.; Park, J.; Varlamov, S.M.; Yoon, J.; Kim, Y.H.; Seo, S.; Park, Y.; Min, H.S.; Lee, J.H.; Kim, C. Seasonal variation of semidiurnal internal tides in the East/Japan Sea. *J. Geophys. Res. Ocean.* **2014**, *119*, 2843–2859. [CrossRef]
99. Lin, F.; Asplin, L.; Wei, H. Summertime M_2 Internal Tides in the Northern Yellow Sea. *Front. Mar. Sci.* **2021**, *8*, 1–15. [CrossRef]
100. Yu, Q.; Pan, H.; Gao, Y.; Lv, X. The Impact of the Mesoscale Ocean Variability on the Estimation of Tidal Harmonic Constants Based on Satellite Altimeter Data in the South China Sea. *Remote Sens.* **2021**, *13*, 2736. [CrossRef]